

**DETC2015-47691**

## **SPRUNG MASS MOTION EMULATION IN A BRAKING TEST RIG**

**Chunjian Wang**  
Clemson University  
Greenville, SC, USA

**Qian Wang**  
Clemson University  
Greenville, SC, USA

**Jeffery Anderson**  
Clemson University  
Greenville, SC, USA

**Beshah Ayalew**  
Clemson University  
Greenville, SC, USA

### **ABSTRACT**

This paper describes a quarter-car braking test rig that includes a hardware-in-the-loop (HIL) means for emulating broader vehicle dynamic effects. The test rig utilizes actual vehicle components such as the suspension-tire assembly and braking system to accurately represent a vehicle during a braking event and a chassis dynamometer's drum is used to simulate the longitudinal vehicle dynamics. The key problem addressed in this paper is the emulation of sprung mass motion with a commercial electromagnetic linear actuator. By accurately representing the motion, detailed effects such as load transfer that happens in a real braking process can be studied for its effect on the braking performance. The stability of the system with sprung mass emulation under different actuator control modes is analyzed. The successful and stable control scheme found is a cascaded control with a velocity tracking strategy. The workings of the test are illustrated via representative test results that include a locked-wheel braking event and a stop with an anti-lock braking system (ABS).

### **1. INTRODUCTION**

Braking performance testing is a very important step in vehicle and tire development since adequate braking is critical to vehicle safety. However, field tests are subject to environment variability which leads to variability in the test results[1] [2]. Brake testing on a drum in a laboratory environment is a good option because it allows for better environment control, avoiding unpredictable factors such as weather, and for easier management of sensor installation/data acquisition.

Several works have looked into the replication of complex braking events in such a laboratory environment. The works presented in [3] and [4] used a brake dynamometer to test brake components during a braking event; however, their method is

not capable of capturing higher level effects such as tire-ground friction, suspension interaction, or sprung mass dynamics. In [5], a variable inertial wheel for a drum dynamometer was proposed so that the full vehicle's braking performance can be tested on it. However, in this case, the vehicle sprung mass is vertically fixed. Therefore, sprung mass dynamics were neglected and load transfer effects during the braking event could not be included. Besides this, the requirement for a whole vehicle prevents this testing in the early stages of vehicle development stages. In [6], a general quarter vehicle test rig was developed with the tire and suspension components of the actual vehicle and with physical weights attached to the top of the suspension to represent the sprung mass. They also suggested the idea of using electromagnetic linear motors to simulate the inertial and aerodynamic loading but no further details were given about the implementation.

In the work we present in this paper, we detail a quarter vehicle braking test rig, where the physical sprung mass is omitted and an electromagnetic linear actuator is used to emulate sprung mass motion. Using a load cell mounted between the actuator and suspension, the dynamic vertical suspension force is measured. This signal is then used to emulate the dynamics of the sprung mass via a quarter car simulation model on real-time computing hardware. A cascaded control scheme is used to drive the actuator and track the simulated desired dynamics of the sprung mass. The stability of the complete test rig is then analyzed under alternative control schemes by using a mathematical model of the test rig. It is found that velocity tracking provides a consistent approach to stabilize the actuator and the test rig.

The advantage of using an actuator instead of a physical sprung mass is that the testing is more flexible with respect to adjustment of the vehicle parameters. With this setup, it is also possible to include vehicle parameters such as position of the

center of gravity height and account for load transfer effects. This paper includes illustrations of how this may be accomplished. It also includes results from both locked-wheel braking and ABS braking to illustrate the effectiveness of the overall control strategy.

The rest of the paper is organized as follows. Section 2 will introduce the hardware configuration of the quarter-vehicle test rig. It will also discuss the overall configuration of the control system. The stability analysis of two possible control strategies considered for implementation of the sprung mass emulation will be presented in Section 3. Test results and discussions are included in Section 4. Finally, the conclusions are given in Section 5.

## 2. CONFIGURATION OF QUARTER-VEHICLE BRAKING TEST RIG

The quarter-vehicle braking test rig is built around the chassis dynamometer at the Clemson University International Center for Automotive Research. The main components of the test rig are shown in Figure 1. The drum of the dynamometer is used to emulate the road surface and inertia of the vehicle to be stopped. The test rig consists of a base fixture, linear guide bearings to accommodate the vertical motion of the sprung mass or top of the suspension, and an adapter plate to accept components from different vehicle's suspension. It also includes components of braking system, including ABS modulators. A load cell is installed between the actuator and suspension to measure the force applied to the top of the suspension by the actuator. The tire/wheel speed sensor and the dynamometer velocity signal are also accessible.

With the control of the vertical movement of the sprung mass enabled by the actuator, the test rig allows us to study complex phenomena related to the braking event. Specifically, the rig can be used to study interactions between various tire and/or suspension designs, or active systems such as ABS, and sprung mass vertical dynamics including load transfer and aerodynamics effects.

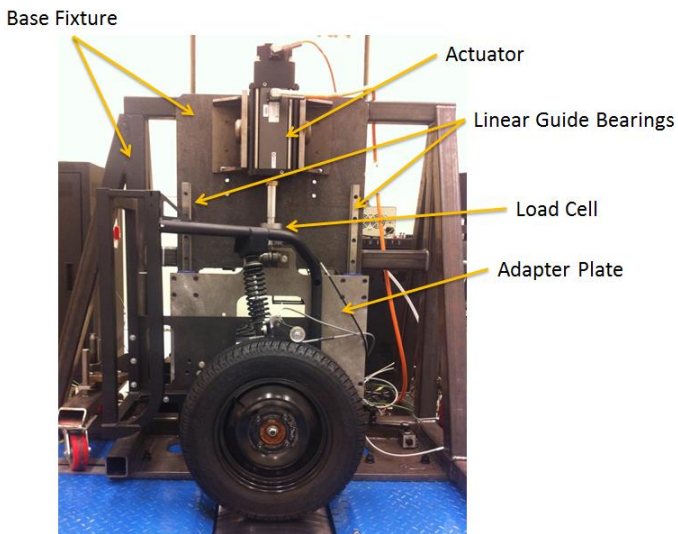


Figure 1: The quarter-vehicle braking test rig with a quarter-vehicle assembly mounted on the chassis dynamometer

The control system of the test rig has two major subsystems: one for sprung mass emulation and the other for braking control. The control scheme for sprung mass emulation is shown in Figure 2. The electromagnetic linear actuator is controlled by a drive module which outputs the command signals to control the position, velocity and force of the actuator. A built-in absolute position encoder provides feedback of the position and velocity of the actuator to its drive module, which consists of the closed internal loop. For the external loop (where mass emulation occurs), dSPACE hardware is used to simulate the sprung mass dynamics via a quarter-vehicle model by applying the measured suspension force as its input. From this computed desired motion dynamics a reference signal is then sent to the drive module to be tracked via the internal control loop.

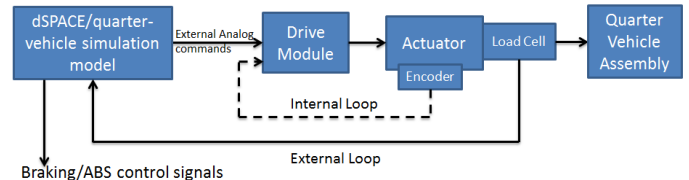


Figure 2: The control scheme for sprung mass emulation

During a braking test, dSPACE also controls the brake actuation and electromagnetic valves in the hydraulic circuits in the ABS module. The components and set up of the braking control system are rather standard; however, the specific details of the brake system and ABS can also be found in [7][8][9].

## 3. SPRUNG MASS EMULATION AND STABILITY ANALYSIS

The key problem and unique feature of this test rig is the emulation of the sprung mass motion via a cascaded two level control. Within the constructs of the linear actuator's drive controller module supplied by the manufacturer, position or velocity tracking are the two possible control modes provided. Therefore, the reference signal supplied to this drive module must be either suspension position or velocity. Both of these can be calculated based on a given sprung mass and the measured vertical load (suspension force) on it in real-time. Then, the desired reference signal can be fed into the drive module's motion control loop (the internal loop). The loop utilizes a PI controller to drive the tracking error to zero.

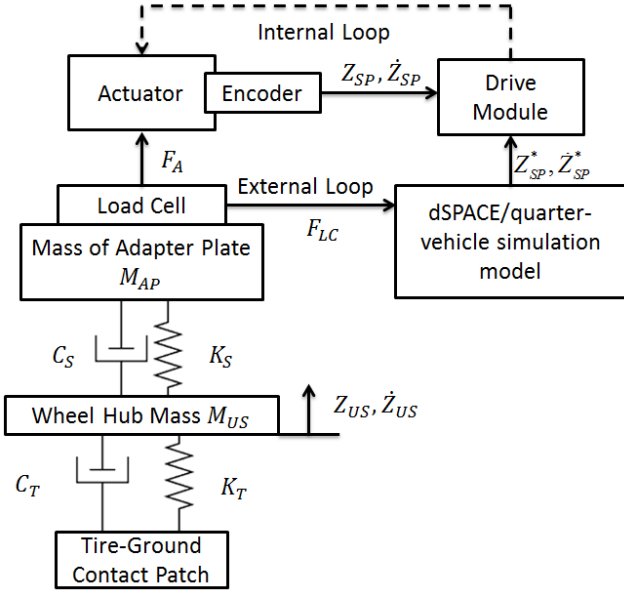


Figure 3: System diagram for sprung mass emulation

The system diagram or model of the sprung mass emulation scheme is shown in Figure 3, where tire-suspension structure of the quarter-vehicle is modeled as a series mass-spring-damper system. As shown here,  $K_T$ ,  $C_T$ ,  $K_S$  and  $C_S$  are tire vertical stiffness and damping, and the suspension vertical stiffness and damping, respectively.  $F_A$ ,  $F_{LC}$  are actuator force and load cell measurement, respectively.  $Z_{SP}$ ,  $\dot{Z}_{SP}$  represents the suspension vertical position and velocity measured by the actuator's built-in encoder. The variables  $Z_{SP}^*$ ,  $\dot{Z}_{SP}^*$  (denoted by the superscript star) represent the desired suspension vertical position and velocity as simulated in dSPACE. The vertical position and velocity of the wheel center (unsprung mass) are represented by  $Z_{US}$  and  $\dot{Z}_{US}$ , respectively. The emulated sprung mass is assumed to be  $M_{sprung}$ , while the unsprung mass is represented by the known constant,  $M_{US}$ . Because the quarter-vehicle suspension will be mounted to the adapter plate in an analogous way as the suspension is mounted to the actual vehicle, the mass of the adapter plate  $M_{AP}$  must be accounted for when specifying  $M_{sprung}$ .

To analyze the dynamics of this system, we consider the model for the sprung mass motion on the test rig. The Equation of Motion (EOM) for the actual sprung mass would be:

$$M_{sprung}\ddot{Z}_{SP} = -K_S(Z_{SP} - Z_{US}) - C_S(\dot{Z}_{SP} - \dot{Z}_{US}) - M_{sprung}g \quad (1)$$

where  $\ddot{Z}_{SP}^*$  is the desired acceleration of the sprung mass.

Due to the rigid connection between the actuator rod, load cell and adapter plate, the three components share the same position, velocity and acceleration; therefore, the motion of emulated sprung mass can be obtained by the following:

$$(M_{sprung} - M_{AP})\ddot{Z}_{SP} = F_A - (M_{sprung} - M_{AP})g \quad (2)$$

For implementation of this emulation in the dSPACE controller hardware, the actuator output force  $F_A$  in equation (2)

is replaced by load cell measurement  $F_{LC}$ . The adapter plate mass,  $M_{AP}$ , is a known constant and with a specified  $M_{sprung}$  and measured actuator force  $F_{LC}$ , the desired acceleration of sprung mass  $\ddot{Z}_{SP}^*$  can be calculated from equation (2). Finally, the desired/emulated velocity  $\dot{Z}_{SP}^*$  and position  $Z_{SP}^*$  of sprung mass can be obtained by integration of  $\ddot{Z}_{SP}^*$  with respect to time.

Similarly, the EOM for the unsprung mass  $M_{US}$  and  $M_{AP}$  are given by:

$$M_{US}\ddot{Z}_{US} = -K_T Z_{US} - C_T \dot{Z}_{US} + K_S(Z_{SP} - Z_{US}) + C_S(\dot{Z}_{SP} - \dot{Z}_{US}) - M_{US}g \quad (3)$$

$$M_{AP}\ddot{Z}_{SP} = F_A - K_S(Z_{SP} - Z_{US}) - C_S(\dot{Z}_{SP} - \dot{Z}_{US}) - M_{AP}g \quad (4)$$

### Stability Analysis for Position Tracking Mode

The control logic of the drive module for position tracking is shown in Figure 4 [10]. In the position tracking mode, the reference signal generated by the external loop/dSPACE controller will be the desired sprung mass position  $Z_{SP}^*$ . This is obtained through twice integration of  $\ddot{Z}_{SP}^*$  in equation (2). Then, the actuator force output  $F_A$  generated by the drive module is given by:

$$F_A = K_{PV}[K_{PP}(Z_{SP}^* - Z_{SP}) - \dot{Z}_{SP}] + K_{IV} \int [K_{PP}(Z_{SP}^* - Z_{SP}) - \dot{Z}_{SP}] dt \quad (5)$$

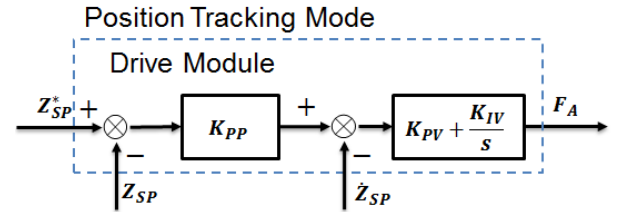


Figure 4: Control logic for position tracking

To put, equation (5) in a convenient state variable form in the analysis to follow, we introduce, auxiliary variables  $Z_I^*$  and  $Z_I$  with:

$$\dot{Z}_I^* = Z_{SP}^* \quad (6)$$

$$\dot{Z}_I = Z_{SP} \quad (7)$$

Substituting (6), (7) into (5) and using  $Z_{SP} = \int \dot{Z}_{SP} dt$  yields:

$$F_A = K_{PV}[K_{PP}(Z_{SP}^* - Z_{SP}) - \dot{Z}_{SP}] + K_{IV}[K_{PP}(Z_I^* - Z_I) - Z_{SP}] \quad (8)$$

Equation (2)(3)(4)(8) comprise a linear system for the cascaded two level position tracking control. Let the closed-loop system states be described by:

$$X_P = [Z_I^*, Z_{SP}^*, \dot{Z}_{SP}^*, Z_I, Z_{SP}, \dot{Z}_{SP}, Z_{US}, \dot{Z}_{US}]^T \quad (9)$$

The state space form of the linear system can be written as:

$$\dot{X}_P = A_P X_P + B_P \quad (10)$$

where the matrices  $A_P$  and  $B_P$  are given by:

$$A_p = \begin{bmatrix} 0 & 0 & -\frac{K_{IV}K_{PP}}{(M_{Sprung} - M_{AP})} & 0 & 0 & \frac{K_{IV}K_{PP}}{M_{AP}} & 0 & 0 \\ 1 & 0 & -\frac{K_{PV}K_{PP}}{(M_{Sprung} - M_{AP})} & 0 & 0 & \frac{K_{PV}K_{PP}}{M_{AP}} & 0 & 0 \\ 0 & 1 & 0 & 0 & 0 & 0 & 0 & 0 \\ 0 & 0 & \frac{K_{IV}K_{PP}}{(M_{Sprung} - M_{AP})} & 0 & 0 & -\frac{K_{IV}K_{PP}}{M_{AP}} & 0 & 0 \\ 0 & 0 & \frac{K_{PV}K_{PP} + K_{IV}}{(M_{Sprung} - M_{AP})} & 1 & 0 & -\frac{K_{PV}K_{PP} + K_{IV} + K_S}{M_{AP}} & 0 & \frac{K_S}{M_{US}} \\ 0 & 0 & \frac{K_{PV}}{(M_{Sprung} - M_{AP})} & 0 & 1 & -\frac{K_{PV} + C_S}{M_{AP}} & 0 & \frac{C_S}{M_{US}} \\ 0 & 0 & 0 & 0 & 0 & \frac{K_S}{M_{AP}} & 0 & -\frac{K_S + K_T}{M_{US}} \\ 0 & 0 & 0 & 0 & 0 & \frac{C_S}{M_{AP}} & 1 & -\frac{C_S + C_T}{M_{US}} \end{bmatrix}^T$$

$$B_p = [0 \quad 0 \quad -g \quad 0 \quad 0 \quad -g \quad 0 \quad -g]^T$$

The stability of the system can then be analyzed by the finding the eigenvalues of  $A_p$  for a given setting of the test rig. That is for the selected tire, suspension and controller settings. For this high order system, closed-forms of the eigenvalue expressions could not be written compactly. However, for the specific set up we considered, the parameters listed in the Appendix can be used for some numerical analysis.

### Stability Analysis for Velocity Tracking Mode

In the velocity tracking mode, the reference for the drive module is the desired sprung mass velocity  $\dot{Z}_{SP}^*$ . The control logic is shown in Figure 5 [10] and output actuator force  $F_A$  is given by:

$$F_A = K_{PV}[\dot{Z}_{SP}^* - \dot{Z}_{SP}] + K_{IV} \int [\dot{Z}_{SP}^* - \dot{Z}_{SP}] dt \quad (11)$$

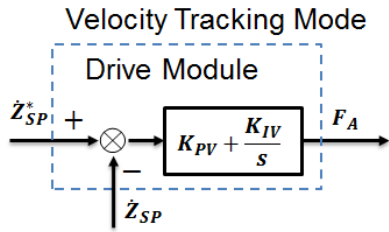


Figure 5: Control logic for velocity tracking

This result differs from (5) in that the integral term in (11) can be written as:

$$\int [\dot{Z}_{SP}^* - \dot{Z}_{SP}] dt = Z_{SP}^* - Z_{SP} \quad (12)$$

Now, (12) can be substituted in to (11), to obtain:

$$F_A = K_{PV}[\dot{Z}_{SP}^* - \dot{Z}_{SP}] + K_{IV}(Z_{SP}^* - Z_{SP}) \quad (13)$$

Combining (2)(3)(4)(13), the linear system for velocity tracking can be written similar to above as:

$$\dot{X}_V = A_V X_V + B_V \quad (14)$$

where the system states are listed as follows:

$$X_V = [Z_{SP}^*, \dot{Z}_{SP}^*, Z_{SP}, \dot{Z}_{SP}, Z_{US}, \dot{Z}_{US}]^T \quad (15)$$

and the  $A_V, B_V$  matrices are given by:

$$A_V = \begin{bmatrix} 0 & 1 & 0 & 0 & 0 & 0 \\ \frac{K_{IV}}{(M_{sprung} - M_{AP})} & -\frac{K_{PV}}{(M_{sprung} - M_{AP})} & \frac{K_{IV}}{(M_{sprung} - M_{AP})} & \frac{K_{PV}}{(M_{sprung} - M_{AP})} & 0 & 0 \\ 0 & 0 & 0 & 1 & 0 & 0 \\ \frac{K_{IV}}{M_{AP}} & \frac{K_{PV}}{M_{AP}} & -\frac{K_{IV} + K_S}{M_{AP}} & -\frac{K_{PV} + C_S}{M_{AP}} & \frac{K_S}{M_{AP}} & \frac{C_S}{M_{AP}} \\ 0 & 0 & 0 & 0 & 0 & 1 \\ 0 & 0 & \frac{K_S}{M_{US}} & \frac{C_S}{M_{US}} & -\frac{K_S + K_T}{M_{US}} & -\frac{C_S + C_T}{M_{US}} \end{bmatrix}$$

$$B_V = [0 \quad -g \quad 0 \quad -g \quad 0 \quad -g]^T$$

The stability of the velocity tracking control is determined by the eigenvalues of  $A_V$ .

### Sprung Mass Emulation with Load Transfer

To include the load transfer in the sprung mass emulation, the deceleration of the drum  $\dot{V}_D$  is used to calculate the load transferred to one corner of the car during braking [11]:

$$W_T = \dot{V}_D \times \frac{Z_g}{a+b} \times \frac{1}{2} M_{VS} \quad (16)$$

where  $V_D$  is the velocity of the drum, which can be obtained from the dynamometer in real-time. In order for the dynamometer to accurately capture the vehicle's inertia for the longitudinal dynamics, the vehicle mass needs to be programmed in dynamometer's controller so that it can be accurately represented.  $Z_g$  is the height of the Center of Gravity (CG) of the vehicle.  $a+b$  equals the total wheel base.  $M_{VS}$  is the mass for the complete vehicle.

Considering the weight transfer effect, the desired sprung mass dynamics of the quarter vehicle is now:

$$(M_{sprung} - M_{AP})\ddot{Z}_{SP}^* = F_{LC} - (M_{sprung} - M_{AP})g - W_T \quad (17)$$

By replacing (2) with (17) in the emulation model in dSPACE controller, sprung mass emulation with load transfer is achieved. Due to the independence of  $W_T$  from any state in  $X_P$  or  $X_V$  indicated by (16), the stability of either position tracking or velocity tracking system will not be changed after introduction of load transfer. Aerodynamic lift effects could be emulated similarly.

## 4. RESULTS AND DISCUSSIONS

### Eigenvalues of the Closed-loop Systems

The matrices  $A_p$  and  $A_V$  are calculated using the parameters listed in Table 2. The damping terms  $C_T$  and  $C_S$  are set to zero. The eigenvalues of the systems are given in Table 1. It can be seen that position tracking has poles in the right half plane and is not stable; however, the velocity tracking controller is stable with all of its poles in the left half plane.

To study the effect of the choice of controller gains, the locus of the real part of the eigenvalues for the position tracking strategy are plotted by varying the values of gain  $K_{PP}$  as shown in Figure 6. The trace number in each figure corresponds to a specific eigenvalue defined in Table 1, and range of  $K_{PP}$  is selected from a very small value to about 240/s considering the capacity of the actuator. It can be seen that even with tuning the

gain  $K_{PP}$  within the given range, the eigenvalues are always in the right half plane. Therefore stability of the system will not be achieved by the choice of the gain  $K_{PP}$ .

The other gains and the velocity tracking strategy can be studied in the same way. It turns out the gain  $K_{PV}$  will not change the stability of the velocity tracking strategy either (as shown in Figure 7) within the studied rang from around  $0.2e6Ns/m$  to around  $2.4e6Ns/m$ . All gain choices leave the system eigenvalues in the left half plane. Therefore, the velocity-tracking mode is always stable for these gain choices.

Table 1. Eigenvalues of the system under different control modes and gain settings

Trace No.	Position Tracking	Velocity Tracking
1	-2634	-6739
2	-63.41	-0.0971
3	$0.0333 + 65.82i$	$-0.0005 + 65.85i$
4	$0.0333 - 65.82i$	$-0.0005 - 65.85i$
5	$0.7239 + 9.445i$	$-0.0045 + 9.587i$
6	$0.7239 - 9.445i$	$-0.0045 - 9.587i$
7	-0.09708	NA
8	$2.842e-14$	NA

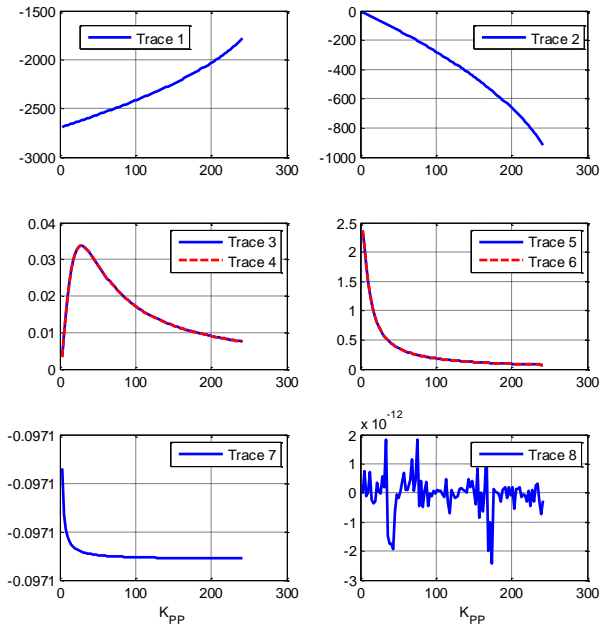


Figure 6: Locus of real part of eigenvalues of  $A_P$

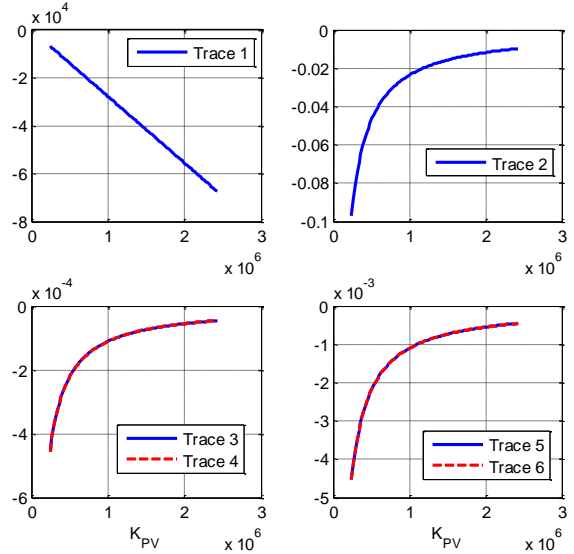


Figure 7: Locus of real part of eigenvalues of  $A_V$

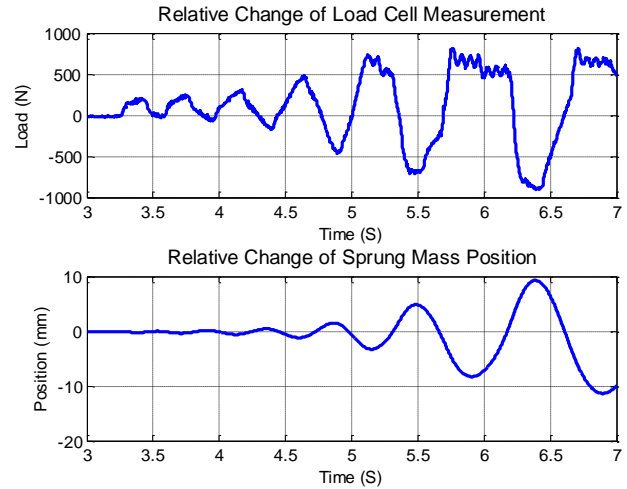


Figure 8: Load cell measurement when equalizing the system via position tracking mode

### Braking Test Implementation

As shown in the above analysis, position-tracking mode is inherently unstable. This instability was observed experimentally when position tracking control is used to find the equilibrium of the system. The actuator is manually set to an arbitrary position then, the position tracking control is turned on expecting to drive the actuator to the equilibrium position of the emulated sprung mass. However, as Figure 8 shows load cell measurement and actuator position are divergent.

In order to demonstrate the effectiveness of the velocity-tracking mode for sprung mass emulation and illustrate the function of the rig, braking tests with and without ABS control were conducted.

Figure 9 shows the results for sprung mass motion emulation with load transfer under locked-wheel braking. It can be seen that after the braking action is applied at around

$t = 28s$ , the wheel velocity drops to 0 in a very short time while the dyno velocity (corresponding to vehicle velocity) drops at a much slower rate. This shows the expected slip between tire and ground in locked-wheel braking. During the braking event, significant load transfers effects were emulated and can be seen in the load and the motion of the actuator.

Figure 10 shows the results for an ABS braking event without load transfer. The dyno and wheel velocity curves show that the ABS stopped the vehicle while preventing the tires from locking-up. As one would expect, no significant load change is observed (since load is being regulated to a fixed value) although it can be seen that the controller did compensate for changes during the test by moving the actuator position in order to precisely control the vertical load.

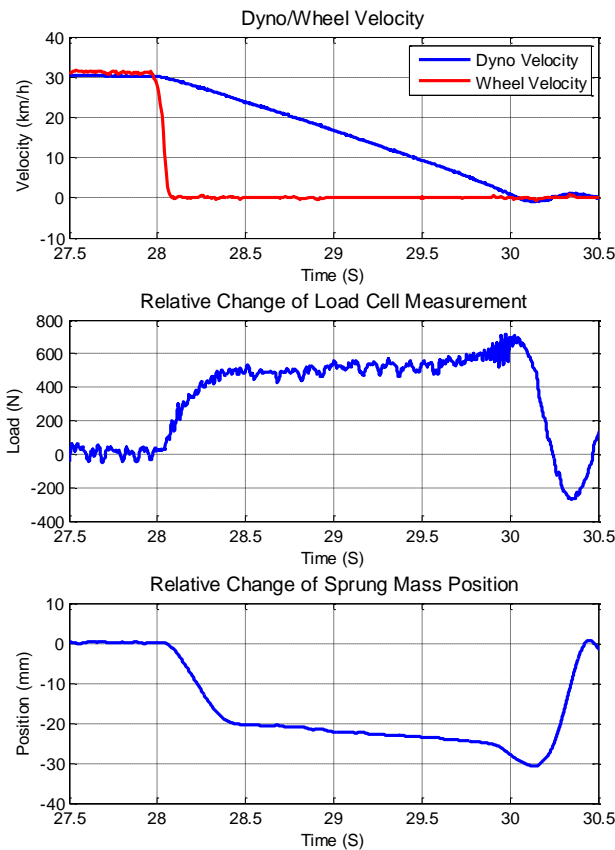


Figure 9: Results of locked-wheel braking with load transfer

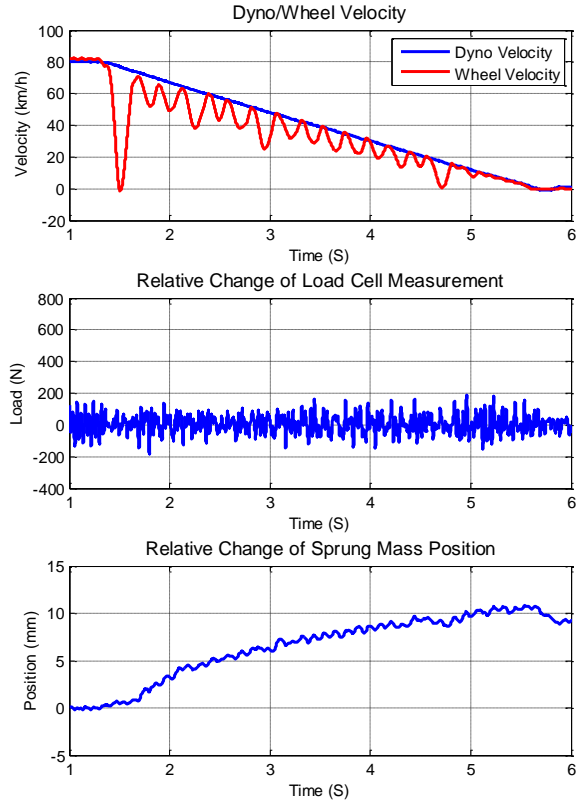


Figure 10: Results of ABS braking without load transfer

## 5. CONCLUSIONS

In this paper, a quarter-car test rig for braking test with sprung mass emulation was introduced. The test rig itself utilizes components from an actual vehicle including the wheel-tire assembly, ABS and braking system, and quarter vehicle suspension. A chassis dynamometer's drum was used to emulate the longitudinal vehicle dynamics. For vertical dynamics, an electromagnetic linear actuator was used to emulate the motion of the sprung mass. To control this actuator, a cascaded two-level control scheme was utilized. Two actuator control strategies are introduced and the stability properties of each were analyzed. It was found that the position tracking strategy is inherently unstable for the full range of possible gain settings. Velocity tracking, however, was shown to be a stable system and successful sprung mass emulation was demonstrated with this control. Both control strategies are implemented on the test rig and the analytical results were corroborated. A divergent result was observed when using the position tracking strategy, which verifies its instability. Sprung mass emulation with and without load transfer for locked wheel and ABS braking were successfully demonstrated using the controller's velocity tracking mode.

## APPENDIX:

Table 2. List of system parameters

Parameters	Unit	Value
$K_{PP}$	1/s	24.168

$K_{PV}$	N*s/m	242640
$K_{IV}$	N/(m*s)	23556
$M_{Sprung}$	kg	150
$M_{AP}$	kg	90
$M_{US}$	kg	40
$K_S$	N/m	15140
$K_T$	N/m	158000

## REFERENCES

- [1] J. Grochowicz, C. Agudelo, A. Reich, K.-H. Wollenweber, and H. Abendroth, "Brake dynamometer test variability part 2-description of the influencing factors," in *SAE 2011 Annual Brake Colloquium and Engineering Display, BRAKE 2011, September 18, 2011 - September 21, 2011*, New Orleans, LA, United states, 2011.
- [2] J. Grochowicz, K.-H. Wollenweber, C. Agudelo, and H. Abendroth, "Brake dynamometer test variability - Analysis of root causes," in *SAE 2010 Annual Brake Colloquium and Engineering Display, October 10, 2010 - October 10, 2010*, Phoenix, AZ, United states, 2010.
- [3] J. K. Thompson, A. Marks, and D. Rhode, "Inertia simulation in brake dynamometer testing," in *20th Annual Brake Colloquium and Exhibition, October 6, 2002 - October 9, 2002*, Phoenix, AZ, United states, 2002.
- [4] J. Ma, B. Wu, X. Liu, and J. Sun, "A new method of inertia simulation in brake dynamometer testing," in *26th Annual Brake Colloquium and Exhibition, October 12, 2008 - October 15, 2008*, San Antonio, TX, United states, 2008.
- [5] Y. Lv, W. He, M. Hou, J. Yao, Z.-a. Qu, Z. Zhu, *et al.*, "Emulation and experimental study of drum dynamometer for simulating the vehicle's road braking," in *2011 International Conference on Measuring Technology and Mechatronics Automation (ICMTMA), 6-7 Jan. 2011*, Los Alamitos, CA, USA, 2011, pp. 37-40.
- [6] J. Langdon and S. C. Southward, "Development of a general use quarter-vehicle test rig," in *19th Int. Conf. Design Theory and Methodology and 1st Int. Conf. Micro and Nano Systems, presented at - 2007 ASME International Design Engineering Technical Conferences and Computers and Information in Engineering Conference, IDETC/CIE2007, September 4, 2007 - September 7, 2007*, Las Vegas, NV, United states, 2008, pp. 1239-1245.
- [7] J. Adcox, B. Ayalew, T. Rhyne, S. Cron, and M. Knauff, "Experimental investigation of tire torsional dynamics on the performance of an Anti-Lock Braking System," in *ASME 2013 International Design Engineering Technical Conferences and Computers and Information in Engineering Conference, IDETC/CIE 2013, August 4, 2013 - August 7, 2013*, Portland, OR, United states, 2013, p. Computers and Information in Engineering Division; Design Engineering Division.
- [8] J. R. Anderson, J. Adcox, B. Ayalew, M. Knauff, T. Rhyne, and S. Cron, "Interaction of a slip-based anti-lock braking system with tire torsional dynamics," in *33rd Annual Meeting and Conference on Tire Science and Technology, The Tire Society, September 8-10, 2014*, Akron, OH, United states, 2014.
- [9] C. Wang, B. Ayalew, J. Adcox, B. Dailliez, T. Rhyne, and S. Cron, "Self-Excited Torsional Oscillations under Locked-Wheel Braking: Analysis and Experiments," in *33rd Annual Meeting and Conference on Tire Science and Technology, The Tire Society, September 8-10, 2014*, Akron, OH, United states, 2014.
- [10] B. Rexroth, "Rexroth IndraDrive MPx-17 Functions Application Manual Edition 03."
- [11] G. Genta, *Motor Vehicle Dynamics: Modeling and Simulation*: World Scientific, 1997.